Linear creep of bonded FRP-strengthened metallic structures at warm service temperatures

Linear creep of bonded FRP-strengthened metallic structures at warm service temperatures

S. Wang[1]*, T. Stratford[1] and T.P.S Reynolds[1]

[1] School of Engineering, Institute for Infrastructure and Environment, The University of Edinburgh
The King's Buildings, Mayfield Road, Edinburgh, Scotland, UK, EH9 3FG
Email: songbo.wang@ed.ac.uk, tim.stratford@ed.ac.uk, t.reynolds@ed.ac.uk
* Corresponding Author

Abstract
Ambient cured epoxy adhesive is widely used for bonding fibre reinforced polymer (FRP) plates to metallic structures. The present paper examines a typical strengthening adhesive to investigate the effect of adhesive thermo-viscoelasticity. The response of the adhesive was determined using a series of tests using the multi-frequency scanning mode of a dynamic mechanical analyser (DMA). The thermo-mechanical properties of the adhesive were then characterised using time-temperature superposition parameters and a Prony series representation for generalised Maxwell creep. The adhesive response was in turn used within two finite element (FE) models to examine the effect of creep in the adhesive at warm temperatures (< 100°C) on the performance of a lab-scale carbon fibre-reinforced polymer (CFRP) plate strengthened steel beam and a real-scale CFRP plate strengthened cast-iron beam respectively. The study found that thermo-viscoelastic creep of the adhesive bonding layer causes an increase in the slip between the FRP and the structure, which could induce damage in the bonded joint and make the CFRP becomes less effective, potentially resulting in failure of the strengthening system during the long-term service. Differential thermal expansion effects can enhance the joint bonding stress and allow the plate to maintain its contribution to the moment capacity of the beam; however, this benefit could be lost when temperature decrease, and the additional irreversible damage caused by the increased joint stress could reduce the effectiveness of strengthening further.

Keywords: Bonded strengthening; Structural adhesive; Creep; Thermo-viscoelasticity; Bond-slip criteria; Differential thermal expansion.

1 Introduction

There is increasing demand for repairing and strengthening ageing infrastructure, and bonded fibre-reinforced polymer (FRP) strengthening is becoming more widely applied to rehabilitate metallic structures. The technique can be advantageous compared to traditional bolted or welded steel plate methods, due to its ease of installation, a high strength-to-weight ratio and resistance to corrosion [1–5].

Bonded FRP strengthening relies upon load transfer from the FRP plate to the metallic substrate through the adhesive joint, which is typically an ambient cured epoxy. There has been a large amount of research into various aspects of the bonded joint between FRP to metallic joints, including surface treatment, dynamic loading (e.g., fatigue, impact, and earthquake), and environmental conditions (e.g., sub-zero temperature, elevated temperature, seawater, and ultraviolet light) [6,7].

This paper examines how the viscoelasticity of the bonding adhesive affects the performance of FRP

strengthening applied to metallic structures, at warm service temperatures. 'Warm' in this paper means temperatures that are expected to be encountered during the normal service of a structure, rather than the 'high' or 'elevated' temperatures that might be experienced during an accidental event such as a fire.

1.1 Background

Load is transferred from the FRP strengthening to the metallic substrate through the adhesive, and is characterised by large concentrated shear and normal ("peel") stresses toward the end of the FRP plate [8]. A number of studies have analysed this bond stress distribution behaviour, mostly by assuming the adhesive layer exhibits linear-elastic properties at ambient temperature [9–11]. Similar linear-elastic bond analyses methods are used in design [2,4].

The economics and practical considerations for large civil engineering structures mean that the adhesive joint is typically cured at ambient temperature. Commonly used ambient-cure structural adhesives have glass transition temperatures (T_g) between 40°C to 70°C, where T_g is characterised by tan δ-peak (the ratio of the storage to loss modulus from a DMA test) [1,3,8]. The glass transition, however, does not occur suddenly at this single characteristic temperature. The transition from a hard, glassy state into a soft, rubbery state takes place over a range of temperatures, and the adhesive starts to lose stiffness and strength at temperatures below the characteristic value of T_g [8,12,13]. This reduction in stiffness and strength is accompanied by viscoelasticity and increased creep as the temperature increases.

Solar heating can result in service temperatures that are close to the glass transition temperature of the adhesive [14,15]. Consequently, the behaviour of the adhesive will be viscoelastic at warm service temperatures, and the linear-elastic bond analysis assumption used in design will not be true.

It is not clear, however, whether the impact of viscoelasticity is detrimental or beneficial to the performance of the adhesive joint at warm temperatures. Creep could have a considerable impact of the FRP strengthened structure's performance in the long-term [16,17]. Creep will result in an increase in the slip between the strengthening plate and the substrate with time, and the viscoelasticity will result in a reduction in the local stress carried within the adhesive layer, and an increase in damage proportion, potentially leading to a joint debonding failure [18]. It is also possible, however, that creep will enable stress redistribution along the length of the plate, and this will be beneficial to the performance of the strengthening [8].

Viscoelasticity has been examined for FRP to concrete adhesive joints by several studies [19–22], although these did not examine the effect of creep upon the long-term performance of the strengthened structure. Zhang and Wang [23] developed a finite element (FE) model for a strengthened concrete beam and found that the axial force transferred from the reinforced concrete (RC) beam to the strengthened FRP plate reduces with time due to viscoelasticity in the adhesive layer, but they did not consider the elevated temperature effects, which could bring more significant reduction in FRP axial force and the corresponding reduction on the effectiveness of the strengthening system.

FRP to metallic adhesive joints are likely to be more susceptible to creep at warm temperatures, because of their higher thermal conductivity and lower specific heat capacity, accompanied by higher stresses in the adhesive joint. The higher stresses in the adhesive joint are due to the larger thickness or stiffness of FRP plate typically required to effectively strengthen a metallic structure in flexure, and because the strength of the adhesive joint is usually not limited by the strength of the substrate (unlike in concrete to FRP joints). Nevertheless, the creep behaviour of FRP to metal adhesive joints has received less attention. De Zeeuw *et al.*[24] examined the creep behaviour of the steel-to-steel lap-shear joint under hygrothermal conditions (40°C air and 40°C distilled water), and Ke *et al.*[25] examined the glass transition behaviour and the bond strength of the CFRP-to-steel joint at elevated temperatures; however, this work did not examine how the behaviour affected the consequence of the local bond performance upon a strengthened structure. Sahin and Dawood [12] conducted experiments that analysed the effect

of warm temperatures upon CFRP strengthened steel beams. Their experiments showed that stress redistribution behaviour could help to prevent debonding failure, but this was based upon an elastic model and did not consider the impact of long-term creep of the adhesive layer. Stratford and Bisby [8] developed a simple elasto-plastic strengthened beam model and demonstrated that under warm temperatures, the reduction in the adhesive stiffness and the differential thermal expansion between the metallic beam and the FRP could result in an increase in slip that eventually causes a runaway debonding failure of the FRP-steel adhesive connection. However, they did not consider creep, either, and recommended that a better viscoelastic model should be built to examine the long-term service performance in depth [26].

The original contribution of this paper is to investigate how FRP strengthened structures are affected by warm temperatures, whether creep is significant for the performance these structures at warm temperatures, and whether it is necessary to examine this in design. This is achieved by (a) experimental characterisation of a typical epoxy adhesive used for bonded and FRP strengthening using a linear viscoelastic constitutive model, and (b) applying this viscoelastic adhesive response to examine how it affects the behaviour of two FRP strengthened metallic beams using finite element analysis.

2 Creep Behaviour of the Structural Adhesive

This study uses a linear viscoelastic model for the adhesive, in which the creep response of the adhesive is independent of the applied stress. Linear viscoelasticity occurs where the applied stress is proportional to the creep strain at a given time, and the linear superposition principle, also known as the Boltzmann superposition principle, holds [27]. Whilst structural adhesives can exhibit nonlinear viscoelastic behaviour [19,28,29], the simpler linear viscoelastic treatment is used here to establish whether creep is significant for FRP-strengthened metallic structures at warm temperature and to identify the need for further study. Nonlinear viscoelasticity is being examined in a subsequent stage of the project, and will be reported in a future paper.

The adhesive in this paper was characterised through a series of dynamic thermal analysis (DMA) tests that are described in section 3. The adhesive response was characterised using a generalised Maxwell constitutive model, after making use of time-temperature superposition to build a master curve from the test results; the background theory is described below.

2.1 Linear viscoelasticity for polymer materials

Figure 1 shows typical creep strain curves $\varepsilon(t)$ of viscoelastic materials at constant stress and temperature. Each is for a value of constant stress, and they are characterised by an instantaneous elastic deformation, followed by viscous creep.

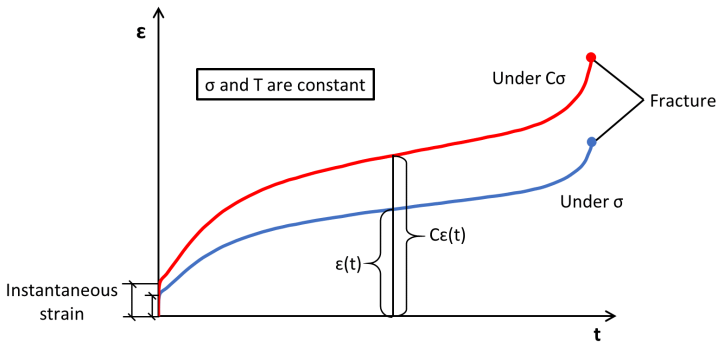

Figure 1. Creep curves for viscoelastic materials

For linear viscoelasticity, the creep behaviour is independent of the stress level, and (as in Figure 1):

$$\varepsilon[C\sigma(t)] = C\varepsilon[\sigma(t)] \quad (1)$$

The creep compliance $D(t)$ can be defined for a linear viscoelastic material as [27]:

$$D(t) = \frac{C\varepsilon(t)}{C\sigma} = \frac{\varepsilon(t)}{\sigma} \tag{2}$$

2.2 Generalized Maxwell model

The generalised Maxwell model is used in this study to characterise the linear viscoelastic response of the adhesive. This consists of an elastic spring ($G_{t=\infty}$) and several parallel Maxwell spring-dashpot elements (G_i, η_i), as shown in Figure 2 [27,30,31].

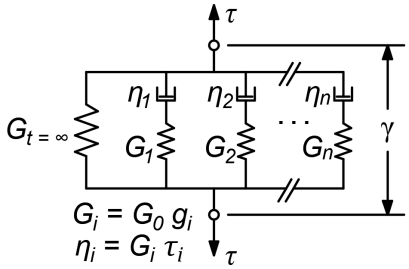

Figure 2. Generalized Maxwell model for linear viscoelasticity

This linear viscoelastic model is expressed as a Prony series, which in section 4 is used as an input to the Abaqus finite element software [30,32,33]:

$$G'(t) = G_0\left[1 - \sum_{i=1}^{n} g_i\,(1 - e^{-t/\tau_i})\right] \tag{3}$$

where $G'(t)$ is the time-dependent shear modulus, G_0 is the initial shear modulus, n is the number of terms in the Prony series, g_i and τ_i are the material parameters. The bulk modulus of the polymer is almost independent of time, so in this study, the corresponding bulk modulus parameters were taken as $k_i = 0$ [33,34], and the time-dependent elastic modulus $E'(t)$ calculated from the time-dependent shear modulus $G'(t)$ and the constant bulk modulus K_0.

Viscoelasticity can alternatively be expressed as a function of frequency, rather than time. This form is used for the dynamic mechanical analysis (DMA) tests that will be used in section 3 to characterise the viscoelastic properties of the adhesive. The frequency domain Prony series is obtained by Fourier transform [30,32–34] (in which $G'(\omega)$ is the frequency-dependent relaxation shear modulus, and ω is the angular frequency):

$$G'(\omega) = G_0\left[1 - \sum_{i=1}^{n} g_i\right] + G_0 \sum_{i=1}^{n} \frac{g_i \tau_i^2 \omega^2}{1 + \tau_i^2 \omega^2} \tag{4}$$

2.3 Time - temperature superposition

The storage modulus of a polymer increases with loading rate but reduces with temperature. For a linear viscoelastic material, different temperatures are observed to result in a sideways shift of the storage modulus vs. frequency curve. The shape of the curve, however, does not change, resulting in the time-temperature superposition principle (TTSP). TTSP allows the viscoelastic response at a low frequency and low temperature to be predicted from the response at a higher frequency and higher temperature [19,27,33].

The DMA tests conducted in this project (section 3) were limited by the frequency range of the analyser, and so TTSP was used to construct a master curve for the adhesive from a series of frequency scans conducted at different temperatures, as shown in Figure 3.

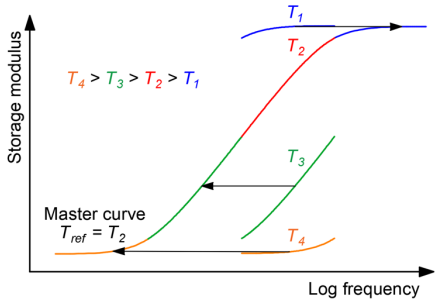

Figure 3. Master curve at the reference temperature $T_{ref} = T_2$ and the unshifted isothermal (T_1-T_4) frequency tests data

The elastic storage modulus curves obtained from tests at different temperatures (T_1 to T_4) are horizontally shifted along the log-frequency scale axis to form the complete master curve at the reference temperature of $T_{ref} = T_2$. The corresponding temperature-dependent shift factors (α_T) are defined by [33]:

$$log(\alpha_T) = log\left(\frac{\omega'}{\omega}\right) \tag{5}$$

where ω is the real applied frequency in the multi-frequency scan tests, and ω' is the shifted frequency used in building the master curve. In this study, those temperature-dependent shift factors (α_T) are described by the Williams-Landel-Ferry (WLF) equation [19,27,33]:

$$log(\alpha_T) = \frac{-C_1(T - T_{ref})}{C_2 + (T - T_{ref})} \tag{6}$$

where C_1 and C_2 are empirical constants, T_{ref} is the reference temperature, and T is the isothermal temperature in each test step.

3 Experimental Characterisation of the Structural Adhesive

A two-part, ambient-cured epoxy was characterised that is used to apply FRP-bonded strengthening in infrastructure projects (Sikadur 330) [35]. A dynamic mechanical analyser (DMA 8000, PerkinElmer) was used to characterise the glass transition response and the viscoelasticity of the adhesive samples at elevated temperatures.

3.1 Test method

The glass transition behaviour of the adhesive was first determined using dynamic mechanical analysis (DMA), using a single cantilever configuration, sinusoidal displacement at 1 Hz, and 2°C/min temperature ramp. The storage modulus, loss modulus and tan δ responses were obtained.

The adhesive was mixed according to the manufacturer's recommendations [35], cast into rectangular adhesive samples (nominally 33 × 7.5 × 1.3mm) , and cured for 7 days at room temperature (nominally 21°C). The DMA specimens and tests were performed in accordance with BS ISO 6721[36].

DMA was used to characterise the glass transition behaviour because it measures the stiffness change of the adhesive, and consequently is of direct relevance to the mechanical performance of the strengthened structure, unlike differential scanning calorimetry (DSC), which measures the temperature-dependent heat flow, or thermomechanical analysis (TMA), which measures dimensional change.

To examine the adhesive's thermo-viscoelasticity, a second set of tests subjected the adhesive samples to multi-frequency strain scans (16 frequencies from 0.01 to 100Hz) in a single cantilever configuration

under isothermal conditions. The applied temperature levels ranged from 25°C to 135°C with a variation of 5°C between two scan steps. The isotherm period of each scan step was set as 1 hour. During that 1 hour, the DMA automatically scanned multiple times at 16 different frequency levels and outputted the average test results. The frequency (time) related storage modulus was obtained at each temperature step and time-temperature superposition principle was used to construct the master curve which could be used to develop the generalised Maxwell model.

3.2 Experimental results

Figure 4 plots the glass transition response of the adhesive in terms of the storage modulus. The T_g test was repeated three times with the independent specimen. The results of each test and its coefficient of variation ($C_{v1\text{-}3}$) are shown in the figure. Meanwhile, two values are shown for the glass transition temperature, T_g [13,36]:

- Onset T_g = 38.0°C, determined from the intersection of two lines tangent to the glassy and leathery portions of the response.
- Peak tan δ T_g = 49.0°C, from the ratio of loss modulus to storage modulus.

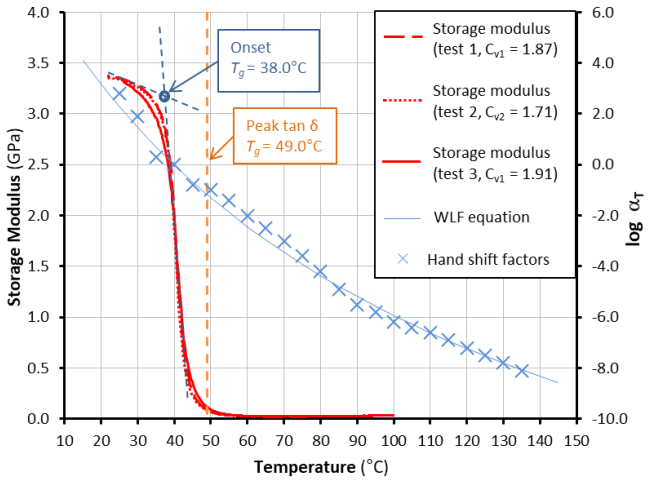

Figure 4. Glass transition response of the adhesive, together with the hand shift factors compared with WLF law prediction

The adhesive's thermal-viscoelastic response is shown in Figure 5. The separate frequency scans conducted at a different temperature are shown, and TTSP was used to construct the master curve at a reference temperature T_{ref} = 40 °C (which was the nearest temperature step to Onset T_g = 38°C).

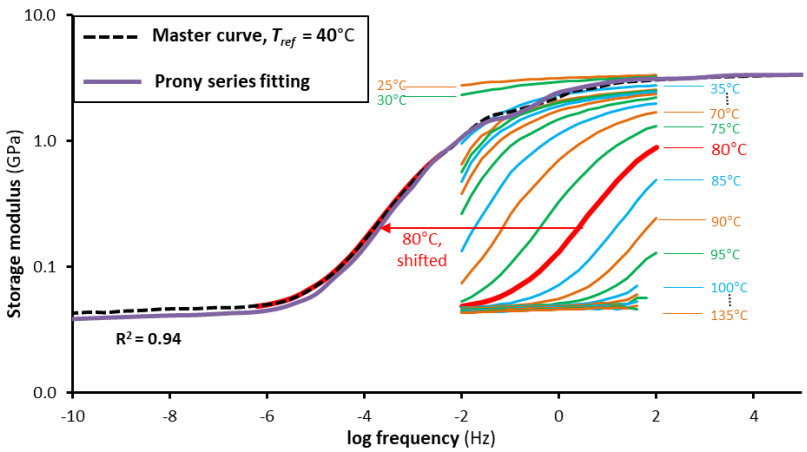

Figure 5. Master curve for T_{ref} = 40°C versus Prony series fitting and the unshifted storage modulus data

3.3 Thermo-viscoelastic material modelling

The shift factors ($\log(\alpha_T)$) required to construct the master curve are shown by the blue crosses in Figure 4, which were fitted using the WLF equation [Eq. (6)] to obtain $C_1 = 21.022$ and $C_2 = 152.64$ (°C). Note that the WLF approach is mainly considered applicable for temperature above T_g [19,27]. As a result, the fitting could be slightly rough in the low temperature range (≤ 40 °C), which corresponds to the relatively high frequency (short time) range (≥ 10^0Hz) of the master curve (in Figure 5).

The master curve was fitted using a 13-term Prony series [Eq. (4)], as shown in Figure 5, and resulting in the parameters given in Table 1.

Table 1. Parameters in the adhesive Prony series

i	g_i	τ_i (s)	i	g_i	τ_i (s)
1	0.0007	4.1×10^{9}	8	0.1511	92
2	0.0001	5.0×10^{8}	9	0.2078	12
3	0.0006	8.2×10^{7}	10	0.3075	0.41
4	0.0006	1.9×10^{6}	11	0.1125	3.9×10^{-2}
5	0.0029	6.7×10^{4}	12	0.0571	9.3×10^{-3}
6	0.0159	6.6×10^{3}	13	0.0695	1.4×10^{-4}
7	0.0628	710×10^{2}	$\sum g_i = 0.9891$		

3.4 Application and limitations of the adhesive constitutive model

Figure 6 plots the adhesive creep compliance curves in the time-domain for three different temperatures, including the $T_{ref} = 40$°C curve. The parameters of the WLF equation fitted as shown in Figure 4 were used to implement the temperature dependence of creep compliance in Abaqus FE software.

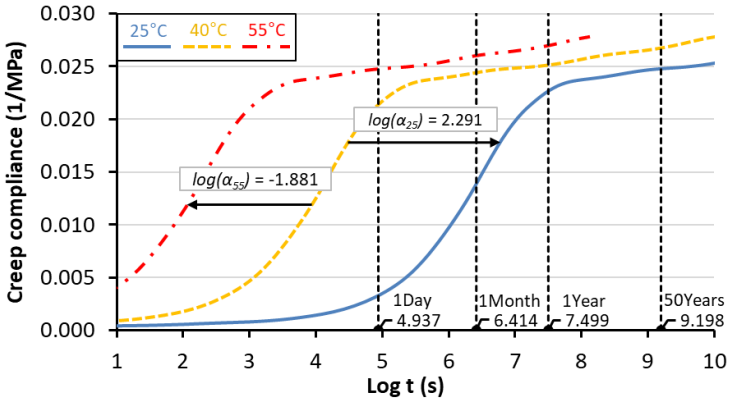

Figure 6. Creep compliance obtained for different temperatures

Dynamic mechanical analysis (DMA) tests and TTSP are convenient for characterising the viscoelastic behaviour of the adhesive in a short time period [26,32,33]. Far longer timescales are of interest for structures to which FRP-bonded strengthening has been applied, which are designed to last for tens of years.

The limitations of using TTSP to extend the DMA test results to such long timescales must be noted. It can be seen from the figure that these timescales are at the edge of the available data; however, it must also be remembered that TTSP assumes linear viscoelasticity, and it has already been noted that the WLF formulation is less accurate below the glass transition temperature. There is currently a scarcity of long-term test data available that can be reliably used to describe the adhesive.

Whilst a more robust viscoelastic model for the adhesive is desirable, the model used here is sufficient for the aim of this project. This was to explore the implications of viscoelasticity on the performance of an FRP-strengthened metallic structure at warm temperatures, and further characterisation of the adhesive was not possible as part of the project.

4 Finite Element Analysis

4.1 Description of the two CFRP-strengthened beams studied

Two metallic beams flexurally-strengthened using bonded FRP were examined using finite element modelling to explore how creep of the adhesive affects their behaviour at warm service temperatures:

- A steel beam with a 2.0m span, as shown in Figure 7.
- A 6.0m span cast-iron beam, shown in Figure 8.

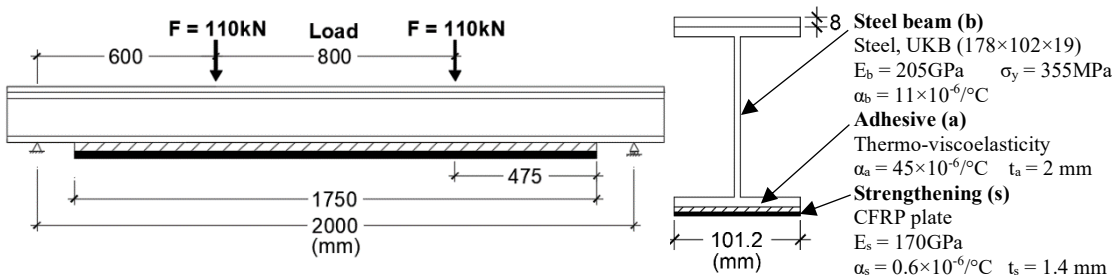

Figure 7. CFRP-strengthened steel beam: geometry and material properties

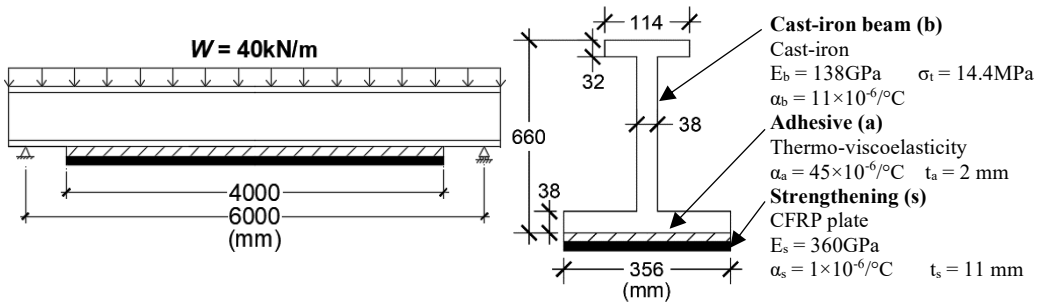

Figure 8. CFRP-strengthened cast-iron beam: geometry and material properties

The CFRP-strengthened steel beam (Figure 7) is similar to the lab-scale configuration tested by Stratford and Bisby [8], but with a top steel plate added avoid premature compression failure. A 2D FE model was constructed using shell (CPS4) elements. The steel was modelled as elasto-plastic (with a yield strength of 355MPa) and the CFRP was purely elastic, using the material properties shown in the figure. The modelling of the adhesive joint is described in the next section.

The cast-iron beam (Figure 8) had been previously been examined by Stratford and Cadei [11] using a linear-elastic bond analysis, and is based upon historic metallic rail bridges described in Cadei *et al.*[2]. The cast-iron beam was modelled in a similar manner to the steel beam, but as cast-iron is brittle, the maximum permissible tensile stress was limited to σ_t = 14.4MPa [2,11]. The CFRP plate was again modelled as purely elastic, but note that a stiffer plate is required to effectively strengthen a cast-iron beam (see the figure), which can result in higher adhesive bond stresses.

The behaviour of the adhesive joint and the performance of the strengthening was examined with time, whilst subject to a constant applied (shown in the figures). A unform temperature was applied to all parts of strengthened beams (steel, adhesive, and CFRP). This temperature was either:

- 25°C being slightly above the cure temperature of the adhesive;
- 40°C, at which the adhesive storage modulus has reduced by around 40% (Figure 4); and
- 55°C, which is above the adhesive's glass transition (Figure 4), but is nevertheless a realistic extreme design service temperature [15].

Note the different coefficients of thermal expansion (α) between the CFRP plate and the metallic beam in both models. Differential thermal expansion can result in substantial bond stresses within the adhesive [2].

4.2 Model for the adhesive joint

The same adhesive joint model was applied to both of the beams. This had two parts:

- The bulk adhesive was modelled using the generalised Maxwell thermo-viscoelastic constitutive model described above.
- The interface between the adhesive and the substrate was modelled using a cohesive model (indicated in Figure 9 and described below).

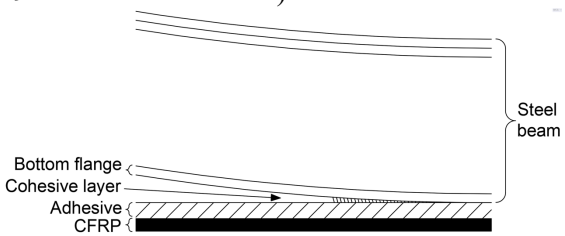

Figure 9. The adhesive joint model

The generalised Maxwell model (Figure 2) was applied to the thickness of the adhesive using the 13-term Prony series characterisation (Table 1), allowing creep of the adhesive to be modelled with temperature. Creep can result in a run-away slip failure in which the adhesive joint is unable to transfer the required load between the strengthening and the beam [2]; however, it does not on its own described the potential debonding of the strengthening from the beam. The cohesive model was required to describe debonding.

The cohesive layer was added between the bottom flange of the metallic beam and the viscoelastic adhesive layer (see Figure 9), as a thin cohesive layer (t_{coh} = 0.01mm). Damage within the cohesive layer was modelled in terms of bond stress *vs.* slip using cohesive elements [30,34]. The temperature-dependent bilinear bond-slip criteria developed by Zhou *et al.*[18] was used, which they obtained from experimental work upon CFRP-to-steel epoxy adhesive joints. This is shown in Figure 10.

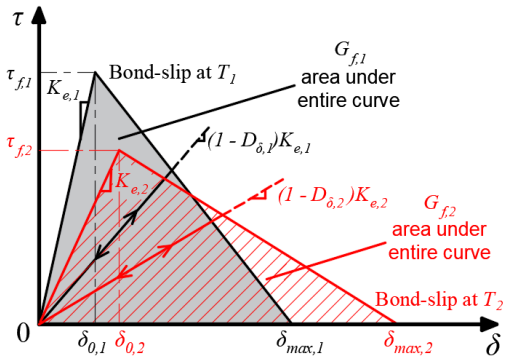

Figure 10. Temperature-dependent bilinear bond-slip relationship

$\tau(\delta)$ is the constitutive law between the shear stress (τ) and interfacial slip (δ), defined in terms of the damage parameter (D_δ) and bond stiffness (K_e) as [5,18,37]:

$$\tau(\delta) = (1 - D_\delta)K_e\delta \quad (7)$$

The damage (D_δ) is the permanent reduction in the bond stiffness and strength of the bonded joint. This is given by the initial slope from Figure 10, and is defined in three parts:

$$D_\delta = \begin{cases} 0 & \delta \le \delta_0 \\ \dfrac{\delta_{max}(\delta - \delta_0)}{\delta(\delta_{max} - \delta_0)} & \delta_0 < \delta < \delta_{max} \\ 1 & \delta_{max} \le \delta \end{cases} \quad (8)$$

The amount of damage increases between $\delta_0 = \tau_f / K_e$ and $\delta_{max} = 2G_f / \tau_f$, in which K_e is the bond stiffness, τ_f is the interfacial shear strength, and G_f is the interfacial fracture energy of the joint [5,18,37].

The three temperature-dependent parameters are:

$$K_{e,t} = \begin{cases} 1785 \times e^{-0.047 T_t} & 20°C \le T_t \le 80°C \\ 98.04 \times e^{-0.011 T_t} & 80°C < T_t \end{cases} \quad (9)$$

$$\tau_f = -0.2428\,T + 21.141\ (\mathrm{N/mm^2}) \quad (10)$$

$$G_f = -0.00206\,T^2 + 0.1978\,T - 2.6185\ (\mathrm{N/mm}) \quad (11)$$

The peak shear stress and fracture toughness parameters were determined by Zhou *et al.*[18]. The elastic stiffness is also based on that determined by Zhou *et al.*, however for the present work it has been modified to allow its use above 80°C, and the time-dependency of the adhesive stiffness has been incorporated by using the shifted temperature, T_t, defined using the WLF equation:

$$-log(t) + log(\alpha_T) = \frac{-C_1\left(T_t - T_{ref}\right)}{C_2 + \left(T_t - T_{ref}\right)} \quad (12)$$

t is the time in seconds, and the parameters are the same as those used in equation (6), for the thermo-viscoelastic material model.

5 The Effect of Creep on the CFRP-strengthened Steel Beam

This section examines how creep affects the behaviour of the lab-scale CFRP-strengthened steel beam (Figure 7).

The results are presented in three stages that allow the viscoelasticity, cohesive layer, and differential thermal expansion effects to be isolated:

- viscoelastic adhesive (but no cohesive layer or differential thermal expansion);
- viscoelastic adhesive and cohesive layer (but no differential thermal expansion); and
- viscoelastic adhesive, cohesive layer, and differential thermal expansion.

5.1 The effect of adhesive thermo-viscoelasticity

Figure 11 plots the distribution of relative slip between the CFRP plate and the soffit of the steel beam, which is the same as the shear deformation across the adhesive. The lower (green) curve in the figure is the elastic bond solution with no creep, with the highest slip at the plate end as expected. The blue, yellow, and red sets of curves report the slips at different sustained temperatures, after 1 day, 1 month, 1 year, and 50 years. The 50-year response was not possible to predict at 55 °C as this was beyond the available adhesive data (see Figure 6).

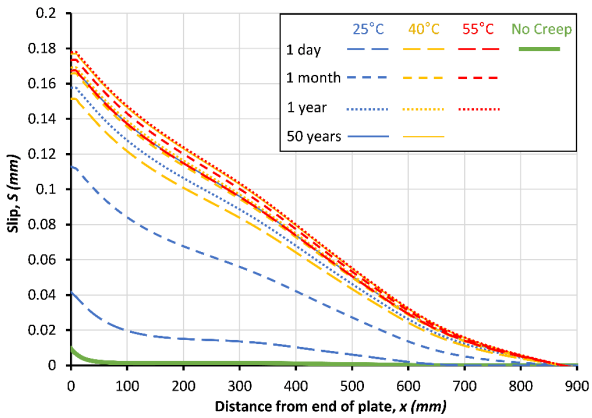

Figure 11. The slip distribution along the strengthened steel beam

Figure 12 plots the CFRP axial stress. As expected, the CFRP axial stress is broadly constant between the loading points (agreeing with a plan sections calculation at mid-span) and increases linearly in the shear span. Close to the plate end the local increase in slip leads to a reduction in the axial stress in the CFRP. Figure 13 plots the axial stress at the bottom of the steel beam, with a particular focus on the central portion of the beam, and shows where yield occurs in the steel.

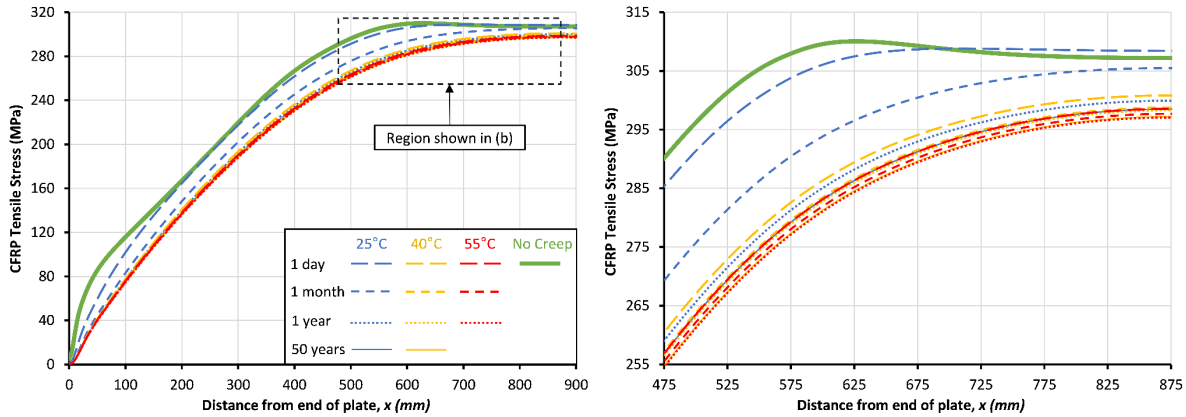

a) Showing half the length of the symmetric beam b) Showing the central portion of the beam in greater detail

Figure 12. CFRP axial stress distribution of the strengthened steel beam

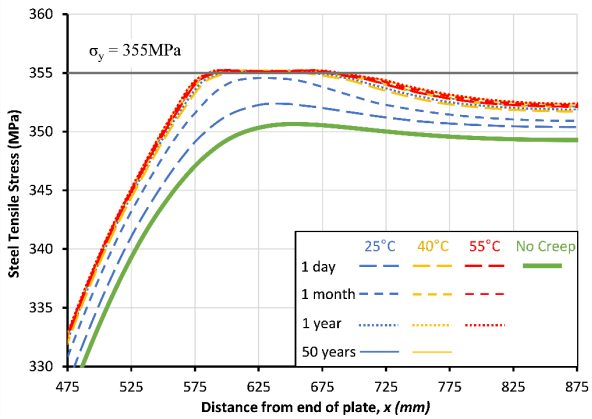

Figure 13. Axial stress at the bottom of the steel beam (central portion).
The higher temperature and time curves are coincident.

Introducing viscoelasticity into the adhesive model results in significant increases in the slip deformation, accompanied by redistribution of the CFRP axial stress along the beam.

- The model predicts that the effects of creep are significant after only 1 day at 25°C. The plate end slip increases from approximately 0.010mm to 0.042mm; however, this does not affect the

load-carrying capacity of the beam because the axial stresses are redistributed along the beam, and the plate stress is unaffected in the central portion of the beam.

- After 1 month at 25°C, the plate end slip has increased substantially to 0.113mm, and the slip distribution affects the centre of the beam. This results in the CFRP stress at the centre of the beam dropping, and consequently the steel beam is required to carry a higher proportion of the moment.
- After 1 year or after 50 years at 25°C, the slip increases further, and the CFRP axial stress reduces. The steel beam must carry more moment, and this means that it starts to yield under the loading points, as shown in Figure 13. Consequently, the strengthening is not able to contribute to carrying the additional continuous loads and is unable to fulfil its function.

Similar behaviour is seen at 40°C and 55°C, but at higher creep rates. For example, a plate end slip of around 0.168mm is seen after 50 years at 25°C, or 1 month at 40°C, or 1 day at 55°C. This results in a reduction in the CFRP plate stress from 290MPa to 257MPa at the loading point (x = 475mm).

5.2 Adding the cohesive joint model to simulate damage

The previous section assumed that the adhesive was perfectly bonded to both the CFRP plate and the steel beam. In this section, the cohesive joint model described above is added to the steel beam model to simulate damage at the interface between the adhesive and the bottom flange of the steel beam.
Figure 14 plots the joint slip and Figure 15 shows the CFRP tensile stress distribution. These can be compared to Figure 11 and Figure 12 in the previous section, and show that the cohesive model results in an increase in slip, a reduction in the load carried by the CFRP strengthening, and consequently a reduction in its effectiveness.

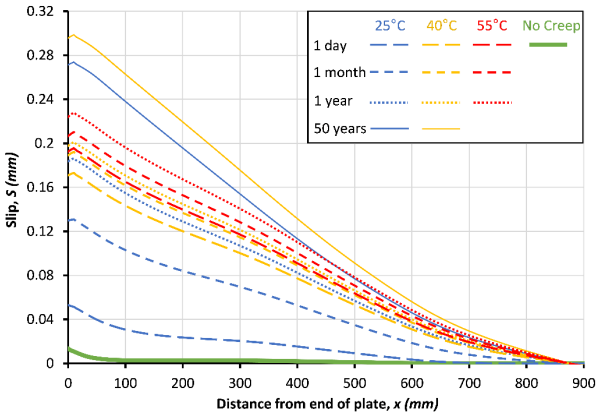

Figure 14. The slip distribution along the strengthened steel beam (with the cohesive layer)

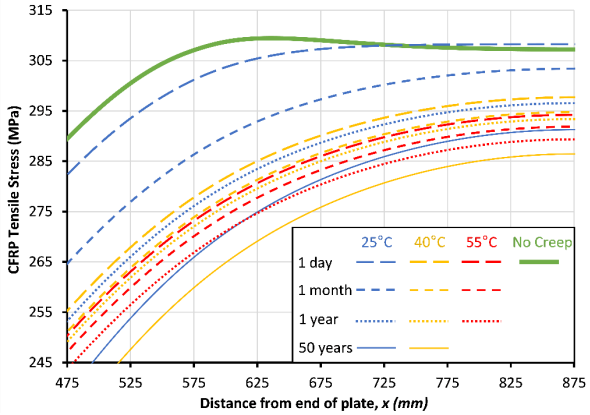

Figure 15. CFRP axial stress distribution in the central portion of the strengthened steel beam (with the cohesive layer)

Figure 16 plots the damage parameter along the adhesive joint (as defined in Eq. (8) and shown in Figure 10). Figure 16 shows that joint damage occurs above 1 month for all three temperatures. The amount of damage is not, however, directly dependent upon temperature, because the fracture energy (G_f) [Eq. (11)] increases with temperature, which enhances the joint deformation capacity [18]. The results show that both the effects of adhesive viscoelasticity and the cohesive layer are important and need to be combined to predict the behaviour of the joint. For the case studied (and for the material properties described above), substantial unrecoverable damage occurs that could affect the effectiveness of the FRP strengthening and bring the risk of debonding failure during long-term service. After 1 year at 25°C, for example, the plate end slip is 0.184mm, and the CFRP stress at the centre of the beam is 298MPa (compared to 0.158mm and 301MPa without the cohesive model). The combined impact of viscoelasticity and the joint damage is likely to be even greater at 50 years, as shown by the substantial region of plate damage in Figure 16.

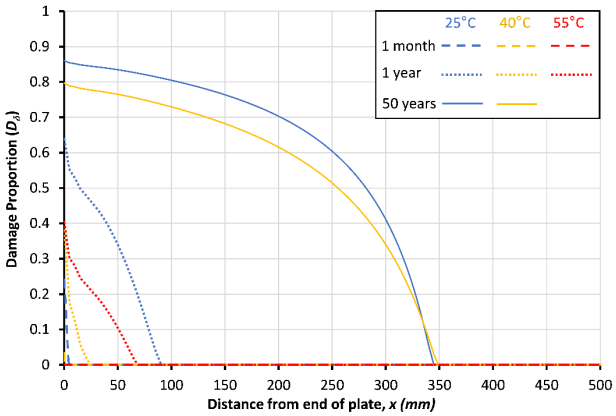

Figure 16. Damage evolution in the CFRP-to-steel bonded joint

5.3 Adding differential thermal expansion

The adhesive viscoelasticity and joint damage described above are material properties. The different coefficients of thermal expansion of the metal beam and the CFRP plate, however, result in thermal mismatch stresses regardless of the material [2]. The coefficients of thermal expansion of the metal beam and the strengthening carbon FRP plate are very different (Figure 7) but were not included in the previous sections. Differential thermal expansion (DTE) effects are now added to the steel beam model. This study assumes that the strengthening was applied to the steel at 25°C.

Figure 17 shows the slip, Figure 18 plots the CFRP axial stress, Figure 19 plots the axial stress in the bottom of the steel beam, and Figure 20 shows the damage parameter. These include “no creep” curves with the elastic solution at each temperature due DTE.

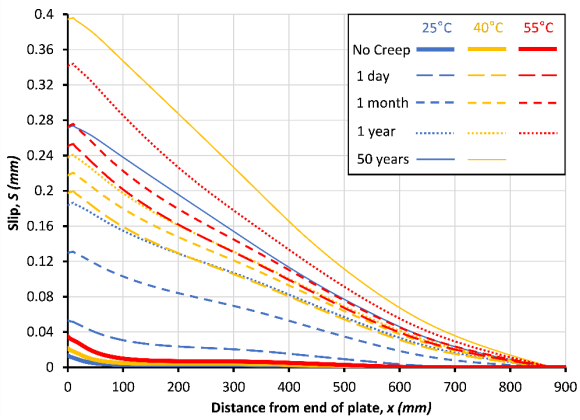

Figure 17. The slip distribution along the strengthened steel beam (including the cohesive layer and DTE)

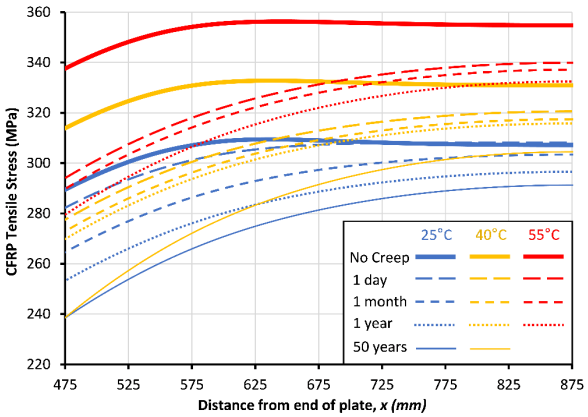

Figure 18. CFRP axial stress distribution in the central portion of the strengthened steel beam (including the cohesive layer and DTE)

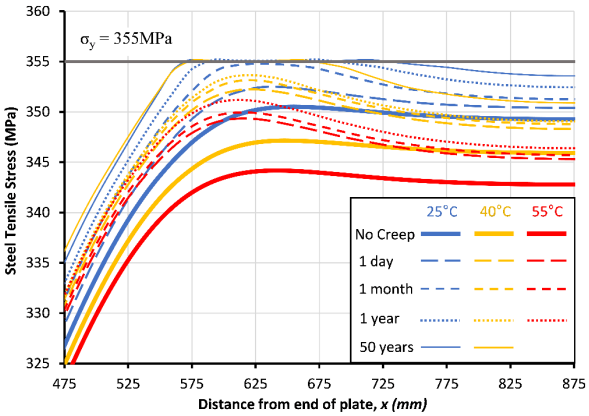

Figure 19. Axial stress at the bottom of the steel beam (central portion, including the cohesive layer and DTE)

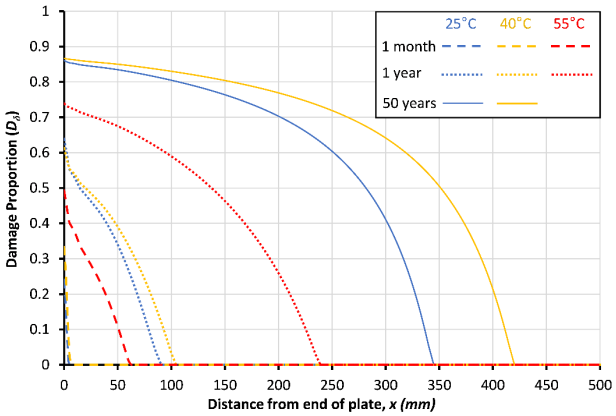

Figure 20. Damage evolution in the CFRP-to-steel bonded joint (including DTE)

The results at 25°C (for which no DTE occurs) are the same as those presented in the last section (Figure 14, Figure 15, Figure 16). The results at 40°C and 55°C, however, are different, due to DTE. This results in higher axial load being carried by the CFRP plate (comparing Figure 18 to Figure 15). The stress in the bottom of the steel beam, however, is lower, so that the steel does not yield. Whilst the effect of DTE appears to be beneficial in these plots, the increased joint damage shown in Figure 20 is irrecoverable when the temperature reduces, so that the DTE will be detrimental when the temperature

returns to the reference temperature, and any benefit is likely to be lost under load or temperature cycles. An analysis of cyclic effects is beyond the scope of the current paper; however, this is currently being undertaken as part of a follow-up study.

Figure 21 shows how the plate-end slip develops with time for different models and temperatures, demonstrating the importance of including viscoelasticity, cohesive damage, and differential thermal expansion within the analysis.

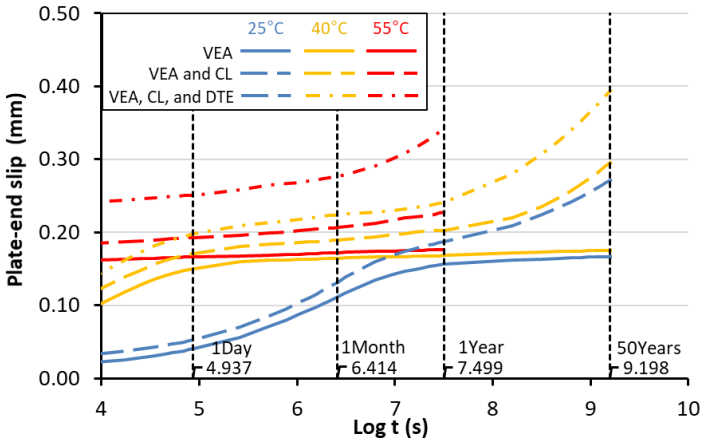

Figure 21. The increase in plate-end slip distribution with time for the three different models

6 The Effect of Creep on the CFRP-strengthened Cast-iron Beam

This section examines how creep affects the behaviour of the CFRP-strengthened cast-iron beam (Figure 8). Whereas the steel beam examined in section 5 was a lab-scale beam subjected to relatively high loads to allow the effects of creep to be examined, the cast-iron beam examined in this section is a real-scale example based upon historic metallic rail bridges and a realistic design scenario [2].

All of the results presented in this section include viscoelastic adhesive and a cohesive layer. Two cases are presented alongside each other, to aid comparison:

- no differential thermal expansion; and
- with differential thermal expansion (with a reference temperature of 25°C).

Figure 22 shows the substantial additional instantaneous shear stresses developed along the adhesive joint as a result of DTE. The maximum plate-end shear stress in the adhesive layer due to load alone is 2.3MPa; however, adding the additional stress caused by the DTE gives a maximum instantaneous shear stress as high as 5.2MPa at 40°C or 7.0MPa at 55°C. This agrees with the elastic distributions previously shown in [2].

Figure 23 shows the plate-end slip distribution, after being subjected to different temperatures and time periods, with no differential thermal expansion on the left compared to with differential thermal expansion on the right. (Note the different vertical scales). The no creep curves correspond to the instantaneous shear stress plots in Figure 22. Figure 24 and Figure 25 similarly plot the distributions of the CFRP axial stress and the bottom flange of the cast-iron beam axial stress along half of the beam.

Without DTE, the slip is relatively low in the strengthened cast-iron beam. It increases under time and temperature from approximate 0.01mm to 0.09mm after 1 year at 55°C. This causes the maximum CFRP stress to reduce from 38.1MPa to 31.6MPa in the middle of the beam, and consequently reduces the effectiveness of the strengthening. The maximum cast-iron axial stress rises from 12.3MPa to 13.7MPa which is only 0.7MPa lower than the permissible maximum tensile stress of σ_t = 14.4MPa.

This a particular concern for brittle cast iron, and demonstrates the potential importance of examining viscoelastic effects when considering warm temperature performance over time.

Including DTE has a substantial impact on the slip, CFRP stress, and cast-iron stress distributions. The 25°C results shown on the right side of the plots agree with those on the left, because this is the referenced temperature and is not impacted by DTE. The 40°C and 55°C distributions, however, are very different, with substantially higher slip, higher axial stresses in the CFRP, and reduced tensile stress in the cast-iron beam. The tensile stress in the middle of the beam decreases to lower than 8MPa at 40°C and 2MPa at 55°C, far lower than the permissible tensile stress.

Differential thermal expansion might be seen as enhancing the strengthening; however, as for the beam the effectiveness of the strengthening will be reduced to creep that is irreversible when the temperature reduces back down to the reference temperature, and under temperature and load cycles (which are being examined in a follow-up study).

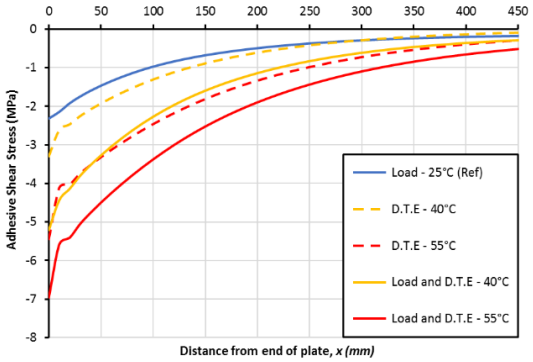

Figure 22. The instantaneous shear stress distribution along the adhesive joint due to applied load and DTE

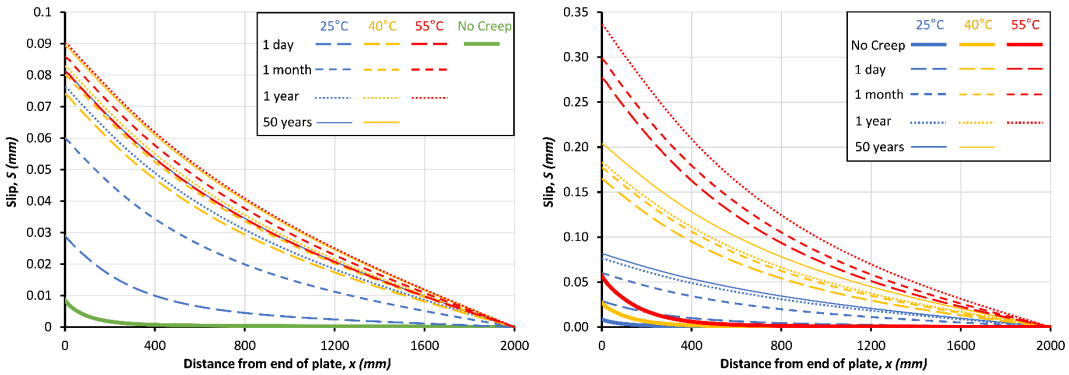

a) not including DTE b) including DTE

Figure 23. The slip distribution along the strengthened cast-iron beam

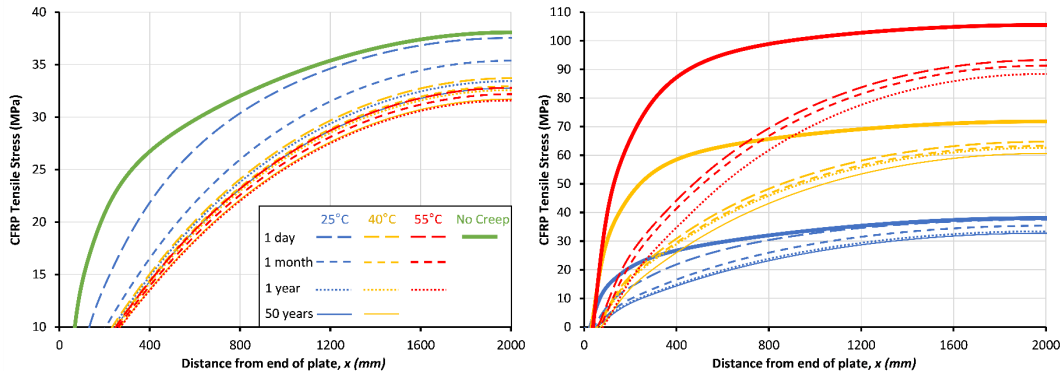

a) not including DTE b) including DTE

Figure 24. CFRP axial stress distribution in the strengthened cast-iron beam

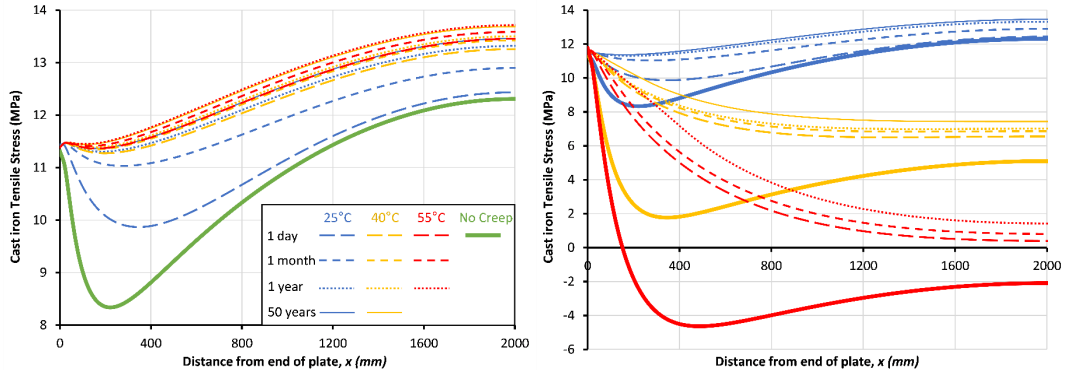

a) not including DTE b) including DTE

Figure 25. Axial stress in the bottom of the cast-iron beam

7 Conclusions

This study demonstrates how creep can have a significant impact upon externally bonded CFRP-strengthened metallic beams subjected to warm service temperatures. The finite element analyses conducted on a laboratory-scale steel beam and a real-scale cast iron bridge beam demonstrate the importance of including thermo viscoelasticity, cohesive debonding, and differential thermal expansion in the model.

The aim of this work is to investigate the impact of linear creep upon CFRP-strengthened beams at elevated temperature, rather than determining a comprehensive characterisation of the adhesive material model. However, a large part of the challenge in this work is to determine the time-dependent material properties required for the adhesive. There is a lack of relevant data available, and the tests are not straightforward to conduct, partly due to the operational lifetime of civil engineering infrastructure. Consequently, a pragmatic approach was taken that combined DMA tests with the time-temperature superposition principle to characterise a typical epoxy strengthening adhesive. Previous tests by Zhou *et al.* [18] were used to describe the cohesive debonding: however, it should be recognised that more testing is needed for a consistent adhesive model that can be applied over long timescales.

Only one type of adhesive has been characterised as part of this work. This adhesive is an ambient-cure epoxy adhesive that is typically used in FRP strengthening. The results of this study are expected to be relevant to other similar adhesives, as long as they are adjusted for the adhesive's glass transition temperature. However, it will be necessary to conduct similar DMA tests to characterise a specific adhesive before applying the method in design.

For the two cases examined, the analytical work shows that adhesive viscoelasticity results in additional slip between the plate and the soffit of the beam. Under increasing time and temperature, the slip will become large, the CFRP stress will reduce, and the strengthening will no longer fulfil its purpose of increasing the moment capacity. This results in greater stress in the beam, and can result in yield in a steel beam, or the brittle rupture of a cast iron beam. This would not be predicted using current elastic design methods.

Differential thermal expansion has a substantial impact upon the strengthened beam. Differential thermal expansion can be beneficial from the perspective of reducing the stress in the metallic beam; however, it places a greater load demand on the strengthening and the adhesive joint, and it can result in creep that is irreversible when the temperature drops back down to the reference temperature.

Comparing the analytical results of the two models, in the lab-scale strengthened steel beam, the applied large loads can cause the greater joint slip and damage, which significantly affect the effectiveness of the strengthening system. In the real-scale strengthened cast-iron beam, the load demand is relatively

low for safety reason; however the increased section dimensions result in significantly greater differential thermal expansion at warm temperatures, which also affects the long-term performance of the beam.

Current design guidance recommends that the T_g (peak tanδ) of the adhesive must be at least 15°C above the operating temperature [1,8]. The adhesive considered here had T_g = 49°C, giving a maximum operating temperature of 34°C; however, it should be noted that viscoelasticity reduces the effectiveness of the strengthening at 25°C.

This paper does not examine the effects of cyclic applied load or cyclic temperatures, which are the subject of a follow-up study. Nevertheless, the analyses presented demonstrate the important of adhesive creep at warm temperatures for bonded FRP strengthening for metallic structures.

CRediT authorship contribution statement

Songbo Wang: Methodology, Formal analysis, Investigation, Writing - original draft, Visualization. **Tim Stratford:** Conceptualization, Resources, Writing - review & editing, Supervision. **Thomas P S Reynolds:** Writing - review & editing, Supervision.

Declaration of competing interest

The authors declare that they have no known competing financial interests or personal relationships that could have appeared to influence the work reported in this paper.

Acknowledgments

This research did not receive any specific grant from funding agencies in the public, commercial, or not-for-profit section. Dr. Colin Robert from The University of Edinburgh is thanked for helping with the experimental work.

References

[1] ACI, ACI 440.2R-08: Guide for the design and construction of externally bonded FRP systems for strengthening concrete structures., Farmington Hills, MI, USA:American Concrete Institute; 2008.

[2] J.M.C. Cadei, T.J. Stratford, L.C. Hollaway, W.G. Dcukett, Strengthening metallic structures using externally bonded fiber reinforced polymer., London, UK: Construction Industry Research and Information Association (CIRIA); 2004.

[3] A. Darby, T. Ibell, J. Clarke, TR55 Design guidance for strengthening concrete structures using fibre composite materials., Surrey, UK: The Concrete Society; 2004.

[4] National Research Council Advisory Committee. Guidelines for design and construction of externally bonded FRP systems for strengthening existing structures – metallic structures., Rome, Italy: National Research Council; 2007.

[5] X.-L. Zhao, FRP-strengthened metallic structures., Boca Raton, FL: Taylor and Francis; 2013.

[6] J.G. Teng, T. Yu, D. Fernando, Strengthening of steel structures with fiber-reinforced polymer composites, J. Constr. Steel Res. 78 (2012) 131–143. https://doi.org/10.1016/j.jcsr.2012.06.011.

[7] X.-L. Zhao, Y. Bai, R. Al-Mahaidi, S. Rizkalla, Effect of Dynamic Loading and Environmental Conditions on the Bond between CFRP and Steel: State-of-the-Art Review, J. Compos. Constr. 18 (2014). https://doi.org/10.1061/(asce)cc.1943-5614.0000419.

[8] T.J. Stratford, L.A. Bisby, Effect of warm temperatures on externally bonded FRP strengthening, J. Compos. Constr. 16 (2012) 235–244. https://doi.org/10.1061/(ASCE)CC.1943-5614.0000260.

[9] S.T. Smith, J.G. Teng, Interfacial stresses in plated beams, Eng. Struct. 23 (2001) 857–871. http://dx.doi.org/10.1016/s0141-0296(00)00090-0.
[10] J. Deng, M.M.K. Lee, S.S.J. Moy, Stress analysis of steel beams reinforced with a bonded CFRP plate, Compos. Struct. 65 (2004) 205–215. https://doi.org/10.1016/j.compstruct.2003.10.017.
[11] T. Stratford, J. Cadei, Elastic analysis of adhesion stresses for the design of a strengthening plate bonded to a beam, Constr. Build. Mater. 20 (2006) 34–45. https://doi.org/10.1016/j.conbuildmat.2005.06.041.
[12] M.U. Sahin, M. Dawood, Experimental Investigation of Bond between High-Modulus CFRP and Steel at Moderately Elevated Temperatures, J. Compos. Constr. 20 (2016) 1–11. https://doi.org/10.1061/(ASCE)CC.1943-5614.0000702.
[13] D. Othman, T. Stratford, L. Bisby, A Comparison of On-Site and Elevated Temperature Cure of an FRP Strengthening Adhesive, in Proceedings of Fibre Reinforced Polymer Reinforced Concrete Structures (FRPRCS11)., UM, Guimarães, 2013.
[14] K.Y. Wong, Instrumentation and health monitoring of cable-supported bridges, Struct. Control Heal. Monit. 11 (2004) 91–124. https://doi.org/10.1002/stc.33.
[15] Highways Agency. Design manual for roads and bridges., London, UK: HM Stationery Office; 1994.
[16] C. Mazzotti, M. Savoia, Stress redistribution along the interface between concrete and FRP subject to long-term loading, Adv. Struct. Eng. 12 (2009) 651–661. https://doi.org/10.1260/136943309789867926.
[17] A. Gullapalli, J.H. Lee, M.M. Lopez, C.E. Bakis, Sustained loading and temperature response of fiber-reinforced polymer-concrete bond, Transp. Res. Rec. (2009) 155–162. https://doi.org/10.3141/2131-15.
[18] H. Zhou, J.P. Torres, D. Fernando, A. Law, R. Emberley, The bond behaviour of CFRP-to-steel bonded joints with varying bond properties at elevated temperatures, Eng. Struct. 183 (2019) 1121–1133. https://doi.org/10.1016/j.engstruct.2018.10.044.
[19] N. Houhou, K. Benzarti, M. Quiertant, S. Chataigner, A. Fléty, C. Marty, Analysis of the nonlinear creep behavior of concrete/FRP-bonded assemblies, J. Adhes. Sci. Technol. 28 (2014) 1345–1366. https://doi.org/10.1080/01694243.2012.697387.
[20] Y. Jeong, M.M. Lopez, C.E. Bakis, Effects of temperature and sustained loading on the mechanical response of CFRP bonded to concrete, Constr. Build. Mater. 124 (2016) 442–452. https://doi.org/10.1016/j.conbuildmat.2016.07.123.
[21] M. Emara, L. Torres, M. Baena, C. Barris, M. Moawad, Effect of sustained loading and environmental conditions on the creep behavior of an epoxy adhesive for concrete structures strengthened with CFRP laminates, Compos. Part B Eng. 129 (2017) 88–96. https://doi.org/10.1016/j.compositesb.2017.07.026.
[22] M.Z. Naser, R.A. Hawileh, J.A. Abdalla, Fiber-reinforced polymer composites in strengthening reinforced concrete structures: A critical review, Eng. Struct. 198 (2019) 109542. https://doi.org/10.1016/j.engstruct.2019.109542.
[23] C. Zhang, J. Wang, Viscoelastic analysis of FRP strengthened reinforced concrete beams, Compos. Struct. 93 (2011) 3200–3208. https://doi.org/10.1016/j.compstruct.2011.06.006.
[24] C. de Zeeuw, S. Teixeira de Freitas, D. Zarouchas, M. Schilling, R. Lopes Fernandes, P. Dolabella Portella, U. Niebergall, Creep behaviour of steel bonded joints under hygrothermal conditions, Int. J. Adhes. Adhes. 91 (2019) 54–63. https://doi.org/10.1016/j.ijadhadh.2019.03.002.
[25] L. Ke, C. Li, J. He, S. Dong, C. Chen, Y. Jiao, Effects of elevated temperatures on mechanical behavior of epoxy adhesives and CFRP-steel hybrid joints, Compos. Struct. 235 (2020). https://doi.org/10.1016/j.compstruct.2019.111789.
[26] S. Wang, T. Stratford, T. Reynolds, Creep of Adhesively-bonded FRP-strengthened Steel Structures at Elevated Temperatures, in Proceedings of the 9th Biennial Conference on Advanced Composites in Construction (ACIC2019)., Birmingham, UK, 2019.
[27] R.M. Guedes, Creep and fatigue in polymer matrix composites., Cambridge: Woodhead Publishing Limited; 2011.
[28] S. Wang, T. Stratford, T. Reynolds, Nonlinear creep of the adhesive bond in FRP-strengthened steel beams, in Proceedings of the Seventh Asia-Pacific Conference on FRP in Structures

(APFIS 2019)., Surfers Paradise, Gold Coast, Australia, 2019.
[29] P. Majda, J. Skrodzewicz, A modified creep model of epoxy adhesive at ambient temperature, Int. J. Adhes. Adhes. 29 (2009) 396–404. https://doi.org/10.1016/j.ijadhadh.2008.07.010.
[30] Abaqus, ABAQUS User's Manual 6.14., ABAQUS Inc, 2014.
[31] S. Jiang, W. Yao, J. Chen, T. Cai, Finite element modeling of FRP-strengthened RC beam under sustained load, Adv. Mater. Sci. Eng. 2018 (2018). https://doi.org/10.1155/2018/7259424.
[32] G.A. Arzoumanidis, K.M. Liechti, Linear viscoelastic property measurement and its significance for some nonlinear viscoelasticity models, Mech. Time-Dependent Mater. 7 (2003) 209–250. https://doi.org/10.1023/B:MTDM.0000007357.18801.13.
[33] M. Abouhamzeh, J. Sinke, K.M.B. Jansen, R. Benedictus, Kinetic and thermo-viscoelastic characterisation of the epoxy adhesive in GLARE, Compos. Struct. 124 (2015) 19–28. https://doi.org/10.1016/j.compstruct.2014.12.069.
[34] E.J. Barbero, Finite Element Analysis of Composite Materials Using Abaqus™., Boca Raton, FL 33487-2742: CRC Press Taylor & Francis Group, 2013.
[35] SIKA, Sikadur®-330 Data Sheet., Sika Construction Chemicals, 2017.
[36] British Standards Institutions, BSI Standards Publication Plastics — Determination of dynamic mechanical properties, BS ISO 6721:2019, (2019). https://doi.org/https://doi.org/10.3403/BSISO6721.
[37] S.H. Xia, J.G. Teng, Behaviour of FRP-to-steel bonded joints, International Symposiumon Bond Behaviour of FRP in Structures (BBFS 2005)., Hong Kong, China, 2005.